Proc. of the Intl. Conf. on Advances In Civil, Structural and Mechanical Engineering- CSME 2014.

ISBN: 978-1-63248-025-5 doi: 10.15224/ 978-1-63248-025-5-28

Dynamically Studying the Effect of Speed and Loading Increases on a Planetary Gear System for Wind Turbines

Kuo Jao Huang ; Jeng Shiun Chen

***Abstract*—Large scale wind turbines must reliably operate in the highly dynamically harsh situation due to varying wind source and grid safety under which the dynamic performance of their transmission lines is especially concerned. Thus, dynamic investigations on the gear system considering the change process of speed and torque are endeavored in order to achieve the strict performance requirements. This study uses a discrete three-dimensional (3D) dynamic model of planetary gear system (PGS) in which gear design parameters can conveniently be incorporated. The model is formulated basing on equivalent springs accounting for the effect of varying meshing stiffness of mating gear or bearing pairs.. In addition, the physical models of bearings, shafts, and housing frames are also included. Then, after assigning torque and speed change in operation, the dynamic transient and steady- state responses of gear system concerning the shifting process of rotation speed and loading are solved. The dynamic contact forces between gear pairs and bearings are resulted. The simulated contact forces of meshing pairs in a PGS compare with the experimental result by NREL. Finally, the dynamic meshing forces under various operation conditions covering the speed and torque increase are analyzed. The result exhibits a larger increase level of speed and load induces server dynamic effect and thus causes a larger maximum contact force.**

***Keywords*—planetary gear system, dynmaic analysis, speed, loading , mehsing force, wind turbine**

I. INTRODUCTION

Planetary gear systems (PGSs) possess the fine features of power density, precision, and noise and vibration and thus are widely applied in vehicles, aircrafts, energies, and robots [1-3]. Recently, with an arising essential role in wind energy, studies on PGS behaviors under dynamic operation conditions are endeavored for facilitation of their transmission design. Especially, dynamic performance of the PGSs under varying excitation PGS is urgently demanded. Both the equivalent discrete and the finite element methods are commonly applied in gear analyses. In dynamics, the equivalent discrete model is welcomed for its simplicity for computing cost in which an equivalent spring is used representing the mesh stiffness between mating gears or bearing pairs. Some of numerous works to obtain the equivalent stiffness of spur gear pairs are referred [4,5]. In addition, Hedlund [6] calculated the tooth deflection of helical gear pairs by combining the Hertzian contact analysis and tooth foundation flexibility [7].

Kuo Jao Huang /Professor
Mechanical Engineering / Chung Hua University
Taiwan,
Jeng Shiun Chen /graduate student

Mechanical Engineering / Chung Hua University
Taiwan

In the gear study, these researchers [8] are also the pioneers in PGS dynamic analysis. Latter, August and Kasuba [9] found that dynamic responses of PGS are critically affected by the variation of the meshing stiffness and fixity design of their sun gears. Kahraman [10] presented a 3D discrete model to investigate the helical PGS dynamics in which modal shapes and dynamic forces resulting from the static transmission error was investigated. Velex and Flamand [11] indicated the stiffness of meshing gear pairs has a more significant effect on planetary dynamic behavior than the other components. In addition, Sadda and Velex [12] considered torsional, flexural, and axial generalized displacements of components basing on the finite element procedure in which a complex planetary gearing was simplified to a twelve degrees of freedom (DOFs) discrete system. In addition, plentiful studies on planetary gear dynamics of a research team in recent years were presented. The authors analyzed the modal behaviors of PGSs including three- and four-planets of equally spacing and diametrical symmetry with planet meshing phase difference or not using linear or nonlinear models. For example, Lin and Parker [13] calculated natural frequencies of PGSs in which the nonlinearity due to meshing stiffness discontinuity of gear pairs was discussed. In the study [14], using the modal analyses and mesh phasing properties, design rules are analytically derived to suppress specific harmonics of plant modal response of a PGS. Recently, using a nonlinear discrete vibration model, Al-shyyab and Kahraman [15] investigated influences of time-varying meshing stiffness, contact ratio, and backlash on the dynamic responses of single-stage In addition, Farshidianfar et al. [16] investigated the nonlinear vibration of single-stage PGS using several analyzing methods in calculating its dynamic spectrum and modal property. Two-dimensional model discrete in discrete models are commonly adopted by which significant deviation from practical condition may occur. Therefore, an approach using a 3D nonlinear and time varying equivalent discrete model intends to benefit gear dynamic analysis.

For a long time, gear transmission is considered highly reliable. However, large challenge is coming with its increasingly essential role in the application of wind energy field. However, low operation reliability is found some lack of them in speed increasing gearboxes. Thus, performance enhancement of gearing is urgently demanded. In general, wind turbines need operating in a dynamically harsh condition due to the wind field condition and electric grid safety consideration. deeper investigation on dynamics of gear systems is required. In this study, an approach using a 3D time varying nonlinear discrete dynamic model is proposed by which the dynamic behavior of a speed increasing helical PGS under dynamic loading excitation will be investigated. Besides, experimental result of a PGS by NREL is used for verification [17]. Finally, the transient contact forces during shifting

Proc. of the Intl. Conf. on Advances In Civil, Structural and Mechanical Engineering- CSME 2014.

ISBN: 978-1-63248-025-5 doi: 10.15224/ 978-1-63248-025-5-28

process of speed and torque change are analyzed by which the effect on the PGS dynamic performance is discussed.

II. CONFIGURATION and Meshing STIFFNESS

Generally, PGSs are constituted by plural external sun-planet gear pairs and internal planet-ring gear pairs. Fig. 1a shows the configuration and components of a PGS which is a stage of speed increasing gearboxes in wind turbines. Fig. 1b is its discrete analysis model. The ring gear is fixed. The input shaft is connected to carrier and the output shaft is connected after the sun gear for power output.

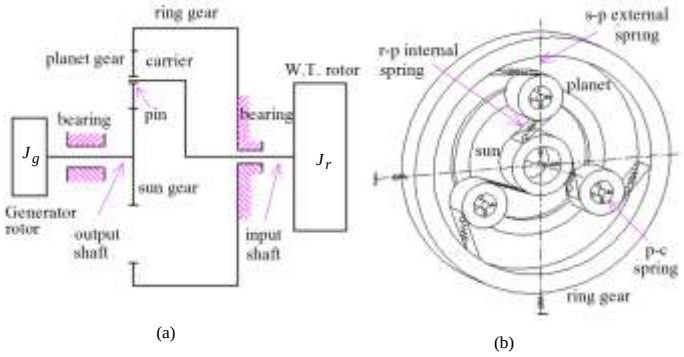

Figure 1. (a) Configuration of PGS; (b) its discrete analysis model

A. Spring for Stiffness of Helical Gear Pairs

The equivalent discrete springs of gear pairs are tangent to the base circles accounting for the varying stiffness of external and internal mating pairs in the PGS as shown in Fig. 2.. Basing on derived involute profile, the stiffness models in this study are obtained by more widely incorporating gear design parameters including tooth number, pressure angle, helical angle, instant contact points, and nonstandard tool setting. k_{si} represents the resulted equivalent stiffness of the *i*th contact tooth pair per face width in the mating spur gears that includes bending deformation of mating teeth, flexible foundation of body [7], and Hertz contact deformation [8]. Basing on the mesh stiffness k_{si} of spur gears, the mesh stiffness $k_{h,i}$ of the *i*th helical tooth pair is expressed as

$$k_{h,i} = \int_0^{L_i} k_{si,j} \cdot dL_{i,j} \tag{2}$$

where $k_{si,j}$ is the stiffness of the *i*th tooth pair per face width for the corresponding equivalent spur gear at instant *j*, $L_{i,j}$ is the length of contact line of the *i*th tooth pair at the *j*th instant. For a helical gear pair with a number n_t of tooth pairs in contact, its equivalent mesh stiffness is

$$k_h = \sum_{i=1}^{n_t} k_{h,i} \tag{3}$$

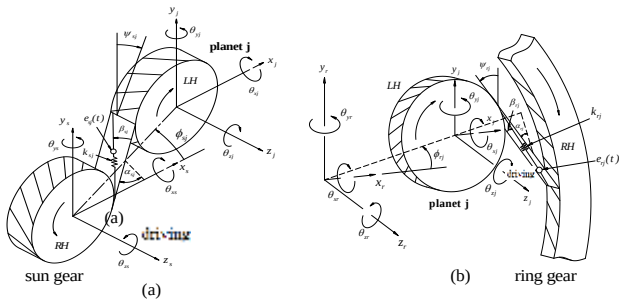

Figure 2. Orientation of stiffness spring of gear pairs: (a) external; (b) internal

B. Hand Sign of Springs of Gear Pairs

Essentially, the geometric and contact force relation of helical gear pairs are much complicated comparing to the spur pairs. The equivalent spring is defined tangent to the base circles of meshing gear, but its orientation is dependent on the driving/driven, helix hand sign, and rotation direction. Fig. 2 shows the orientation of the equivalent spring and the helical gear pairs under a condition. Fig. 2a illustrates the spring for a driving sun gear of right hand (RH) at counterclockwise (CCW) rotation. Once that change rotation direction, orientation angles and tangent points of the spring are changed. The angle of $\psi_{s,j}$ between contact line and y axis is expressed as

$$\psi_{s,j} = \begin{cases} \alpha_{s,j} - \phi_{s,j}, & \text{torque on sun gear is CCW} \\ -(\alpha_{s,j} + \phi_{s,j}), & \text{torque on sun gear is CW} \end{cases} \tag{4}$$

In addition, the orientation of the spring for internal pair is shown in Fig. 2b. Their angle of $\psi_{s,j}$ between contact line and y axis is expressed as

$$\psi_{r,j} = \begin{cases} \alpha_{r,j} - \phi_{r,j} & \text{torque on planet gear is CCW} \\ -(\alpha_{r,j} + \phi_{r,j}) & \text{torque on planet gear is CW} \end{cases} \tag{5}$$

III. GEAR DYNAMIC EQUATIONS

A. *Lagrangian for PGS*

The discrete dynamic model of a PGS is derived using Lagrange equation. The three action pairs which are sun-planet gear pair, planet-ring gear pair, and planet-pin bearing pair are included, respectively. After the additional components of input and output shafts, bearings, housing, and boundary conditions added, the dynamic equation of the PGS can be resulted. The Lagrange equation for resulting dynamic equation is written as

$$\frac{d}{dt}\left(\frac{\partial L}{\partial \dot{q}_i}\right) - \frac{\partial L}{\partial q} = Q_i \tag{6}$$

Proc. of the Intl. Conf. on Advances In Civil, Structural and Mechanical Engineering- CSME 2014.

ISBN: 978-1-63248-025-5 doi: 10.15224/ 978-1-63248-025-5-28

where Lagrangian $L = T - V$ in which T is total kinetic energy, V total strain energy, q_i generalized coordinates, and Q_i generalized forces. Thus, kinetic energy T is the sum of kinetic energy of all the components. For the PGS, that is

$$T = T_{ss} + T_r + \sum_{j=1}^{N_p} T_j + T_c + T_s + T_{cs} \tag{7}$$

in which T_{cs}, T_c, T_j, T_r, T_s, T_{ss} is the componential kinetic energy of the input shaft, carrier, planet gears, ring gear, sun gear, and output shaft, respectively. By considering the translational and rotational displacements of the six DOFs for each part, the energy of the components in the PGS can be expressed as

$$\begin{aligned}
T_{ss} &= \frac{1}{2}[I_{ssx}\dot{\theta}_{ssx}^2 + I_{ssy}\dot{\theta}_{ssy}^2 + J_{ss}(\omega_{ss} + \dot{\theta}_{ssz}^2)] + \frac{1}{2}m_{ss}\left(\dot{x}_{ss}^2 + \dot{y}_{ss}^2 + \dot{z}_{ss}^2\right) \\
T_r &= \frac{1}{2}[I_{rx}\dot{\theta}_{rx}^2 + I_{ry}\dot{\theta}_{ry}^2 + J_r(\omega_r + \dot{\theta}_{rz}^2)] + \frac{1}{2}m_r\left(\dot{x}_r^2 + \dot{y}_r^2 + \dot{z}_r^2\right) \\
T_j &= \frac{1}{2}[J_{jx}\dot{\theta}_{jx}^2 + J_{jy}\dot{\theta}_{jy}^2 + J_{jz}(\omega_j + \dot{\theta}_{jz}^2)] + \frac{1}{2}m_j\left[\dot{x}_j{}^2 + \dot{y}_j{}^2 + \dot{z}_j{}^2\right] \\
T_c &= \frac{1}{2}[J_{cx}\dot{\theta}_{cx}^2 + J_{cy}\dot{\theta}_{cy}^2 + J_{cz}(\omega_c + \dot{\theta}_{cz}^2)] + \frac{1}{2}m_c\left[\dot{x}_c{}^2 + \dot{y}_c{}^2 + \dot{z}_c{}^2\right] \\
T_s &= \frac{1}{2}[I_{sx}\dot{\theta}_{sx}^2 + I_{sy}\dot{\theta}_{sy}^2 + J_s(\omega_s + \dot{\theta}_{sz}^2)] + \frac{1}{2}m_s\left(\dot{x}_s^2 + \dot{y}_s^2 + \dot{z}_s^2\right) \\
T_{cs} &= \frac{1}{2}[I_{csx}\dot{\theta}_{csx}^2 + I_{csy}\dot{\theta}_{csy}^2 + J_{cs}(\omega_{cs} + \dot{\theta}_{csz}^2)] + \frac{1}{2}m_{cs}\left(\dot{x}_{cs}^2 + \dot{y}_{cs}^2 + \dot{z}_{cs}^2\right)
\end{aligned} \tag{8}$$

in which I_* are the moments of mass for the components, * is a dummy symbol for shortening of the text description; J_* are the polar second moments of mass for the components; m_* are mass, ω_* are the angular velocity of rigid body motion. Also, $\dot{\theta}_*$ are the angular velocity and $\dot{x}_*$, $\dot{y}_*$, $\dot{z}_*$ are the translational velocity of elastic deformation. The subscripts * of *s*, *r*, *c*, *j* are the sun gear, ring gear, planet carrier, and the *j*th planet gear.

Next, the total strain energy V including all components in the PGS is written as

$$V = V_{cs} + [\sum_{j=1}^{N_p}(V_{cj} + V_{rj} + V_{sj})] + V_{ss} \tag{9}$$

where V_{cs}, V_{cj}, V_{rj}, V_{sj}, V_{ss} is the componential strain energy of the input shaft, planet-pin pairs, ring-planet pairs, sun-planet pair, and output shaft, respectively. The strain energy of the three kinds of mating pairs are given as

$$\begin{aligned}
V_{cj} &= \frac{1}{2}(k_{xcj}\delta_{xcj}^2 + k_{ycj}\delta_{ycj}^2 + k_{zcj}\delta_{zcj}^2 + k_{\theta_{xj}}\theta_{xcj}^2 + k_{\theta_{yj}}\theta_{ycj}^2 + k_{\theta_{zj}}\theta_{zcj}^2), \\
V_{rj} &= \frac{1}{2}k_{rj}\delta_{rj}{}^2, \\
V_{sj} &= \frac{1}{2}k_{sj}\delta_{sj}^2
\end{aligned} \tag{10}$$

where k_* denote the equivalent stiffness of gear pairs and bearing pairs; δ_{rj} and δ_{sj} are the relative displacement of contact line diagonally tangent to the base circles of mating internal and external gear pairs; d_{xcj}, d_{ycj}, and d_{zcj} are the relative translation displacement of planet-pin bearing pairs; θ_{xcj}, θ_{ycj}, and θ_{zcj} are the relative angle displacement of planet-pin bearing pairs.

B. *Dynamic Equation of PGS*

By using the Lagrange equation in Eq. (6) and incorporating the degrees of freedom (DOFs) of rigid body of the gear system, the equation of motion can be written as

$$\mathbf{M}_1\ddot{\mathbf{X}}_1 + \mathbf{C}_1\dot{\mathbf{X}}_1 + \mathbf{K}_1\mathbf{X}_1 = \mathbf{F}_1 \tag{11}$$

The subscript **1** denotes the equation used for a single stage planetary gear system. $\mathbf{M}_1$, $\mathbf{C}_1$, $\mathbf{K}_1$, and $\mathbf{F}_1$ are the system mass, damping, stiffness, force terms, respectively. Also the displacement vector $\mathbf{X}_1$ of the gear system is written as $\mathbf{X}_1 = \begin{bmatrix}\mathbf{x}_s & \mathbf{x}_r & \mathbf{x}_1 & \mathbf{x}_2 & \dots & \mathbf{x}_{n_p} & \mathbf{x}_c & \mathbf{x}_R\end{bmatrix}$. Each individual elemental vector $\mathbf{x}_* = \begin{bmatrix}x_* & y_* & z_* & \theta_{x_*} & \theta_{y_*} & \theta_{z_*}\end{bmatrix}^{\mathrm{T}}$. Then, the degrees of freedom corresponding to the elastic deformation $\mathbf{x}_f$ and rigid body motion $\mathbf{x}_R$ are separately expressed as

$$\begin{bmatrix}\mathbf{M}_{ff} & \mathbf{M}_{fR} \\ \mathbf{M}_{Rf} & \mathbf{M}_{RR}\end{bmatrix}\begin{bmatrix}\ddot{\mathbf{X}}_f \\ \ddot{\mathbf{X}}_R\end{bmatrix} + \begin{bmatrix}\mathbf{C}_{ff} & 0 \\ 0 & 0\end{bmatrix}\begin{bmatrix}\dot{\mathbf{X}}_f \\ \dot{\mathbf{X}}_R\end{bmatrix} + \begin{bmatrix}\mathbf{K}_{ff} & 0 \\ 0 & 0\end{bmatrix}\begin{bmatrix}\mathbf{X}_f \\ \mathbf{X}_R\end{bmatrix} = \begin{bmatrix}\mathbf{F}_f \\ \mathbf{F}_R\end{bmatrix} \tag{12}$$

In this process, only the rotational degree of freedom corresponding to the z axis rigid body motion is considered. Other DOFs of rigid body motion are stationary. Therefore, the sub-matrices of system mass matrix are given as

$$\begin{aligned}
\mathbf{M}_{ff} &= \mathrm{diag}\begin{bmatrix}\mathrm{m}_{ss} & \mathrm{m}_s & \mathrm{m}_r & \mathrm{m}_{p1} & \dots & \mathrm{m}_{pN_p} & \mathrm{m}_c & \mathrm{m}_{cs}\end{bmatrix} \\
\mathbf{M}_{Rf} &= \mathbf{M}_{fR}{}^{T} \\
&= \begin{bmatrix}\mathbf{0} & \varepsilon_{sc}I_{ss} & \mathbf{0} & \varepsilon_{sc}I_s & \mathbf{0} & \frac{\varepsilon_{sc}}{\varepsilon_{sr}}I_r & \mathbf{0} & \frac{\varepsilon_{sc}}{\varepsilon_{sp,1}}I_{p1} & \dots & \mathbf{0} & \frac{\varepsilon_{sc}}{\varepsilon_{sp,N_p}}I_{pN_p} & \mathbf{0} & I_c + \sum_j^{N_p} m_{pj}r_c^2 & \mathbf{0} & I_{cs}\end{bmatrix}
\end{aligned} \tag{13}$$

$$\mathbf{M}_{RR} = \varepsilon_{sc}{}^2(I_{ss} + I_s) + \sum_j^{N_p}\{(\frac{\varepsilon_{sc}}{\varepsilon_{spj}})^2 I_{pj} + m_{pj}r_c{}^2\} + (I_c + I_{cs}) + (\frac{\varepsilon_{sc}}{\varepsilon_{sr}})^2 I_r$$

in which **0** mean $\mathbf{0}_{1\times5}$ vector is the other 5 DOFs of rigid body motion other the rotational DOF about z axis. Also, speed ratios of gears are defined as $\varepsilon_{sc} \equiv \omega_s / \omega_c$, $\varepsilon_{sr} \equiv \omega_s / \omega_r$. $\mathbf{K}_{ff}$ in Eq. (12) is the discrete stiffness matrix of the PGS model in Fig. 1.

C. *Implementation of Excitation*

Fig. 3 is a time chart of *y*(t) representing the dynamic excitations including the gross motion effect. Its implement on the governing equation of the PGS is described below.

Proc. of the Intl. Conf. on Advances In Civil, Structural and Mechanical Engineering- CSME 2014.

ISBN: 978-1-63248-025-5 doi: 10.15224/ 978-1-63248-025-5-28

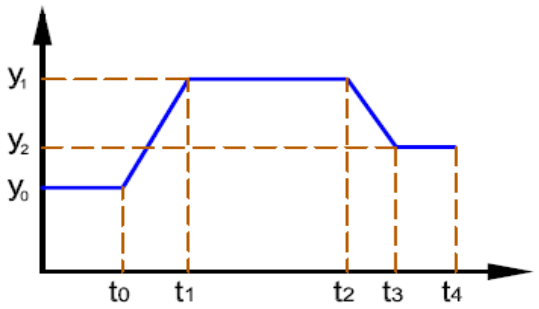

Figure 3. Time-chart for dynamic excitation for gross motion

Excitation vector $\mathbf{F}_1$ in Eq. (11) includes the transmitted torque, inertial force from gross motion, and transmission error. How the gross motion effect included is explained. Eq. (12) is rewritten as

$$\mathbf{M}_{ff}\ddot{\mathbf{X}}_f + \mathbf{M}_{fR}\ddot{\mathbf{X}}_R + \mathbf{C}_{ff}\dot{\mathbf{X}}_f + \mathbf{K}_{ff}\mathbf{X}_f = \mathbf{F}_f \quad (14)$$

$$\mathbf{M}_{Rf}\ddot{\mathbf{X}}_f + \mathbf{M}_{RR}\ddot{\mathbf{X}}_R = \mathbf{F}_R \quad (15)$$

Case 1: For acceleration, $y = \ddot{\mathbf{X}}_R$, corresponding to the gross motion given, dynamic elastic displacement $\mathbf{X}_f$ can be obtained by directly using numerical integration on Eq. (14) as

$$\mathbf{M}_{ff}\ddot{\mathbf{X}}_f + \mathbf{C}_{ff}\dot{\mathbf{X}}_f + \mathbf{K}_{ff}\mathbf{X}_f = \mathbf{F}_f - \mathbf{M}_{fR}\ddot{\mathbf{X}}_R \quad (16)$$

Case 2: For applied force, $y = \mathbf{F_R}$ given, corresponding to gross motion given, Eq. (15) can be rewritten as

$$\ddot{\mathbf{X}}_R = \mathbf{M}_{RR}^{-1}(\mathbf{F}_R - \mathbf{M}_{Rf}\ddot{\mathbf{X}}_f) \quad (17)$$

Substituting Eq. (17) to Eq. (14) yields

$$(\mathbf{M}_{ff} - \mathbf{M}_{fR}\mathbf{M}_{RR}^{-1}\mathbf{M}_{Rf})\ddot{\mathbf{X}}_f + \mathbf{C}_{ff}\dot{\mathbf{X}}_f + \mathbf{K}_{ff}\mathbf{X}_f = \mathbf{F}_f - \mathbf{M}_{fR}\mathbf{M}_{RR}^{-1}\mathbf{F}_R \quad (18)$$

IV. RESULTS AND DISCUSSION

The PGS of three planets shown in Fig. 1 is one stage of the speed increasing gearbox in a 2.2MW wind turbine. The gear data of the PGS are: teeth numbers of gears z^s =19, z^p =34, and z^r =89. The normal module m_n = 16mm, normal pressure angle $\alpha_n = 20°$, helical angle $\beta = 7°$, face width b=330mm. The discrete analysis models of the PGS is shown in Fig. 1b.

A. *Dynamic Response of PGS*

The transmitted torque of 3×10^5 Nm from wind force is exerted on the input shaft coupling with the carrier. The moment inertia J_r on the input shaft is 15kg·m^2 and which on the sun gear is J_g = 0.25kg·m^2. The inertial effect due to gross motion is also considered. The speed-time chart illustrated in Fig. 3 represents the rotation speed and its change process of the input shaft. The PGS is starting up at the time instant of t_0 from the initial speed of ω_0 . Then, it undergoes a constant acceleration or deceleration and achieving the maximum speed of ω_1 at time t_1. Next, a constant speed is maintained until to the time of t_2. After that, it enters to a constant deceleration to the speed of ω_2 at time t_3. At the final period, the PGS runs at ω_2 until to the end of t_4. In this analysis, the starting time t_0 =0. Also, time ratios α_i are defined as: $\alpha_1 = t_1/t_4$, $\alpha_2 = (t_3 - t_2)/t_4$, $\alpha_3 = t_3/t_4$, and $\alpha_4 = (t_4 - t_3)/t_4$. Thus, if the accelerating time ratio $\alpha_1 = 0$, it will be an extreme case of the most impact stepwise up. In this study, the operation speeds of this analysis are assigned as ω_1 =20rpm and $\omega_0 = \omega_2$ =0 rpm. The total operation time is t_4 =0.2s. Besides, $\alpha_1 = \alpha_2$, α_3 = 0.6. Many levels of accelerating time ratio of the speed-time chart is given as α_1 =0.01～ 1.0 for discussion of acceleration effect.

Basing on the above data, the six DOFs of translational and angular displacements of the second planet gear of three settings of $\alpha_1 = 0.04$, 0.09, and 0.16 are shown in Fig. 4. Obviously, decrease of accelerating ratio α_1 causes larger response amplitude on the six DOFs of dynamic displacements. Less values of α_1 imply the PGS is starting up more abruptly. Therefore, the least α_1 which is the largest acceleration has the largest amplitude owing that the severest dynamic effect is induced during the speed increase process.

Furthermore, the action forces in the mating pairs of gears or bearing are also calculated. Fig. 5a and 5b are the contact forces corresponding to the s-p and the r-p gear pairs, respectively. Fig. 5c is the bearing meshing forces in the p-c bearing pairs. The tendency of dynamic contact forces is similar to that in the above dynamic displacements. The most abrupt starts up of $\alpha_1 = 0.01$ induces the severest dynamic effect for all the three mating pairs. The sun-planet pair has a largest peak force of 5.11×10^5N for α_1 = 0.01 that is larger than the forces of 3.16×10^5N and 3.04×10^5N for α_1 = 0.04 and 0.09, respectively. In the r-p pair, it has a largest peak force of 5.18×10^5N for α_1 = 0.01 that is larger than 3.01×10^5N and 3.26×10^5N of other two conditions. Finally, the p-c pair, has a largest peak force of 11.82×10^5 N for α_1 = 0.01 which is larger than that of 5.77×10^5N and 5.85×10^5N for α_1 = 0.04 and 0.09, respectively. As the above described, it demonstrates a smaller acceleration ratio α_1 induces a larger dynamic force. It is rational that a sudden speed change causes more significant dynamic effect. Until now, it shows the dynamic transient and steady-state responses of PGS can be obtained using the proposed 3D discrete model in which many design parameters can effectively be incorporated.

B. *Result Verification by a NREL's PGS*

For verification, an numerical result using the proposed method is compared with the experimental result of a PGS developed by NREL [18]. Fig. 6 shows they have close mean values. The result of the study can be basically verifies.

Proc. of the Intl. Conf. on Advances In Civil, Structural and Mechanical Engineering- CSME 2014.

ISBN: 978-1-63248-025-5 doi: 10.15224/ 978-1-63248-025-5-28

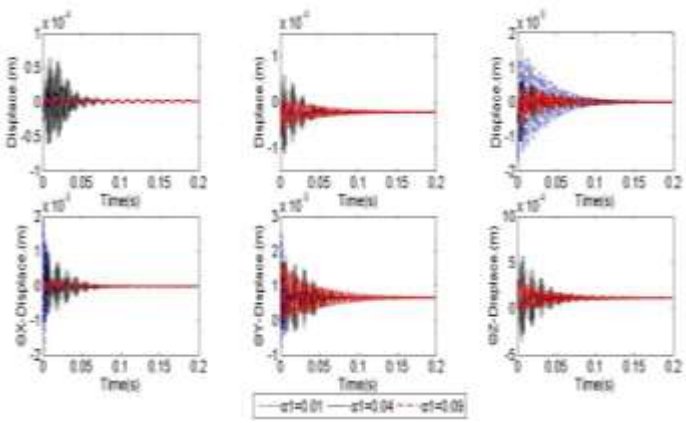

Figure 4. The dynamic displacements of the second planet gear of three kinds of acceleration ratios

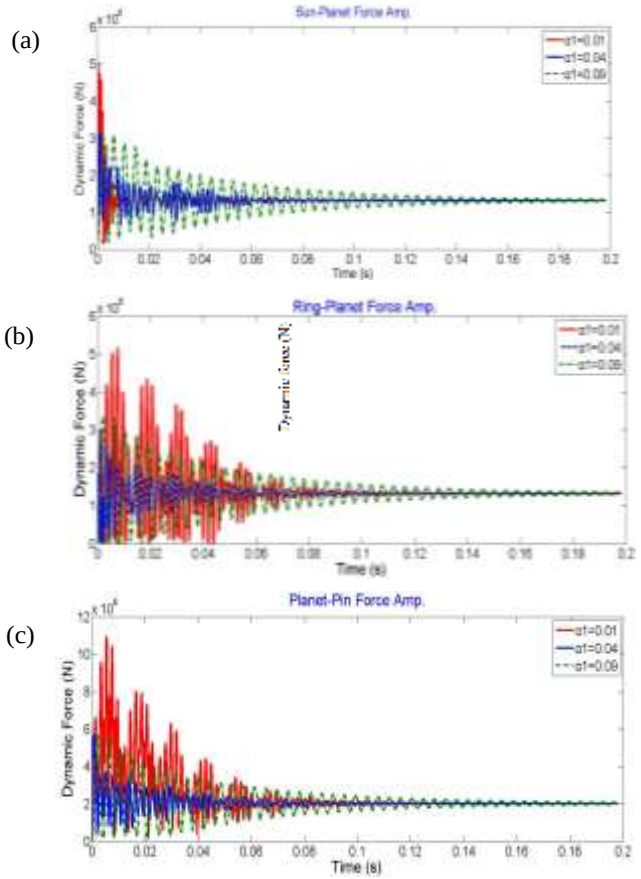

Figure 5. The action forces of mating gear and bearing pairs: of three various acceleration ratios: (a) s-p pair; (b) r-p pair; (c) p-c pair

C. *Result Verification by a NREL's PGS*

For verification, an numerical result using the proposed method is compared with the experimental result of a PGS developed by NREL [18]. Fig. 6 shows they have close mean values. The result of the study can be basically verifies.

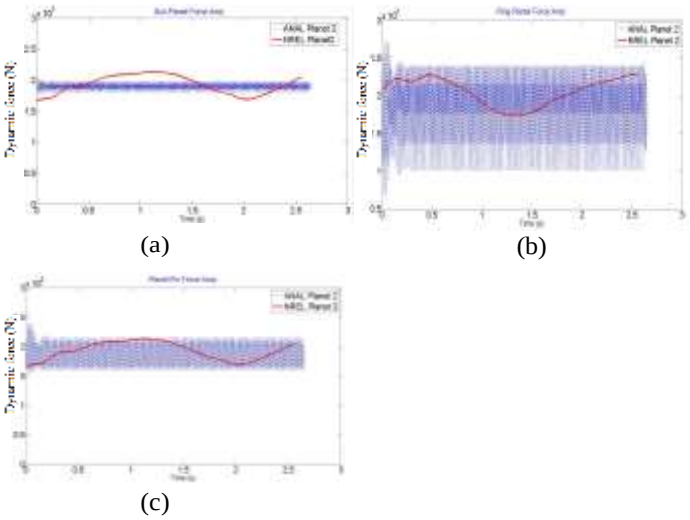

Figure 6. Analysis contact forces of meshing pairs of a PGS compare with the experimental results of NREL: (a) s-p pair; (b) r-p pair; (c) p-c pair

D. *Dynamic Effect of Speed Change*

The dynamic effect of the PGS caused by rotation speed increase from the stalling condition increased to the rating speed is again discussed. That is the initial speed of gearing ω_0 = 0 rpm. Then, the PGS speeds up to $\omega_1 = 22.2$ rpm with different acceleration time ratios. The damping ratio of the gear system is 0.05. The time ratios are $\alpha_3 = 1$ and $\alpha_2 = \alpha_4 = 0$. There are ten accelerating levels of time ratio, $\alpha_1 = 0.01 \sim 1.2$, given in the simulation. Fig. 7 shows the dynamic action forces of mating pairs under various α_1 between the second planet-gear with the sun-gear. It demonstrates that a less value of α_1 induces a larger dynamic force. The figure shows the largest peak force of 5.11×10^5N for α_1 = 0.01 that is larger than 3.16×10^5N and 3.04×10^5N, and 2.28×10^5N for the case α_1 = 0.04, 0.09 and 0.16, respectively. Fig. 8 depicts the all maxima of the dynamic forces of the various α_1 in the s-p, r-p, and p-c pairs. The result again demonstrates a small value of α_1 leads to a large dynamic force since a more sudden speed increase causes a more significantly dynamic effect.

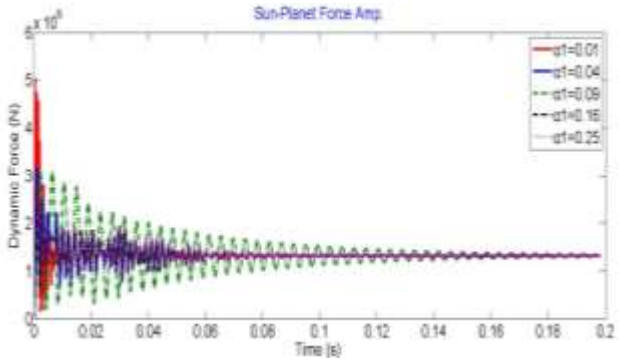

Figure 7. The dynamic contact forces of s-p pair of the 2nd planet gear under five kinds of time ratio settings (α_1)

Proc. of the Intl. Conf. on Advances In Civil, Structural and Mechanical Engineering- CSME 2014.

ISBN: 978-1-63248-025-5 doi: 10.15224/ 978-1-63248-025-5-28

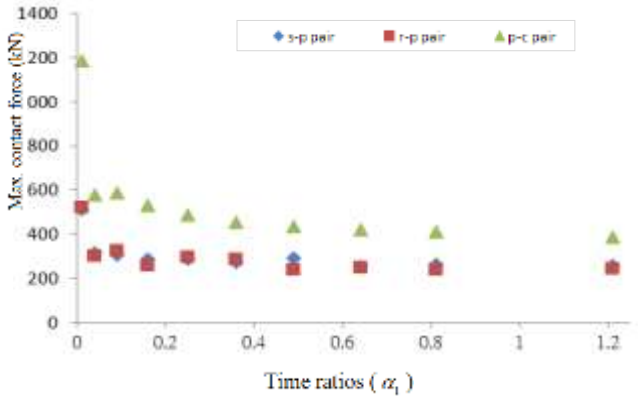

Figure 8. The maxima of dynamic contact forces of s-p pair of under three kinds of time ratio settings (α_1)

E. *Dynamic Effect of Load Change*

The dynamic characteristic of the PGS causing by loading change for operation consideration is finally discussed. The rotation speed ω_1 =22.2 rpm. Here, five kinds of initial input torque T_r are given as 0, 50, 100, 200, and 300kNm. At the beginning, the analysis is done by assigning the initial torque and achieving the PGS response to a steady-state. Then, the PGS is increased to the rating torque of 3.226kNm. Fig. 9 shows the dynamic meshing forces of one of s-p gear pairs under three different conditions of initial torques which are 0, 100, and 200kNm, respectively. It is observed that significant fluctuation of the dynamic responses appear right after the time instant of torque increase. Also, the condition of smaller initial torque shows a server fluctuation and larger dynamic force. It induces a largest peak contact force of 3.29×10^5N for T_r = 0.0kNm that is larger than 3.17×10^5N and 2.61×10^5N for T_r =100 and 200kNm, respectively. The loading condition from 0kNm increasing to 3.226kNm causes the largest dynamic contact force. Fig. 10 is the maxima of dynamic meshing forces for s-p pair, r-p pair, and p-c pair of the five kinds of initial loadings to the rating loading. The result shows that a smaller initial loading has a larger maximum of dynamic force which exhibits rational. A larger level of torque loading change causes a more extreme load fluctuation and induces a severer dynamic effect. The results can be useful of wind turbines subject to the dynamic environment during the design or operation phrases.

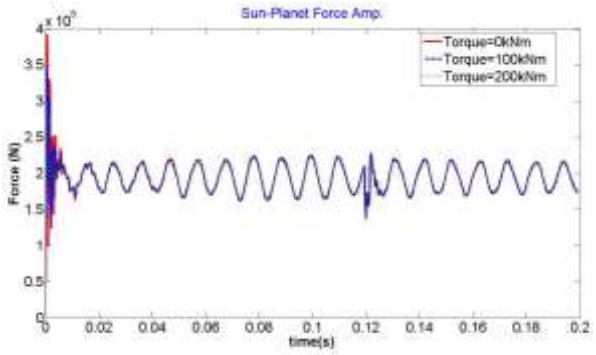

Figure 9. The dynamic contact forces of s-p pair of initial applied torques (T_r)

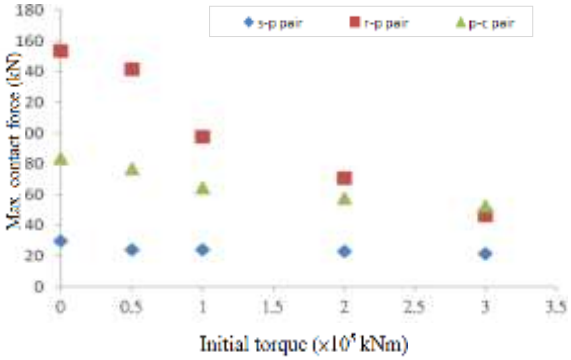

Figure 10. The maxima of dynamic contact forces of s-p pair of various initial applied torques (T_r)

V. CONCLUSIONS

This study used a 3D discrete dynamic model of a helical PGS in wind turbines under dynamic excitations concerning the effect of change process of transmitted loading and rotation speed. The dynamic contact forces between gear pairs and planet bearings were resulted. The discrete analysis model is formulated basing on the equivalent springs for representation of the varying meshing stiffness of mating gear or bearing pairs. The physical models of bearings, shafts, and housing frames were also incorporated. After torque and rotation speed assigned, dynamic transient and steady-state responses of the PGS including the change process of speed and loading were analyzed. The dynamic contact forces between gear pairs and bearings were resulted. The analyzed contact forces of meshing pairs of a PGS compared with the experimental result by NREL. Finally, the transient meshing forces and the maxima of them under different conditions were discussed. The results shows that a sudden level of speed increase leads to serious dynamic fluctuation. Also, a larger loading increase can cause a more significant dynamic contact force. The effect of shift process of speed and loading change on dynamic contact forces demonstrated in this investigation. The obtained result can be used for the wind turbines subject to the dynamic excitation condition during the design or operation phrases.

Proc. of the Intl. Conf. on Advances In Civil, Structural and Mechanical Engineering- CSME 2014.

ISBN: 978-1-63248-025-5 doi: 10.15224/ 978-1-63248-025-5-28

Acknowledgment

The authors would like to thank the financial support from the National Science Council of Taiwan, R.O.C. under grant NSC-102-2221-E-216-004.

References

[1] C. Yuksel and A. Kahraman, "Dynamic Tooth Loads of Planetary Gear Sets Having Tooth Profile wear," Mechanism and Machine Theory, Vol. 39, pp. 695-715, 2004.

[2] A. Bajer and L. Demkowicz, "Dynamic Contact/ impact Problems, Energy Conservation, Planetary Gar Trains," Computer Methods in Applied Mechanics and Engineering, Vol. 191, pp. 4159-4191, 2002.

[3] R. B. Parker and J. Lin, "Mesh Phasing Relationships in Planetary and Epicyclic Gears," ASME Journal of Mechanical Design, Vol. 126, pp.365-370, 2004.

[4] S. Du, R. B. Randall, and D. W. Kelly, "Modeling of spur gear mesh stiffness and static transmission error," Proc. IMechE, Part C: J. Mechanical Engineering Science, vol. 212(4), pp 287-297, 1998.

[5] M. H. Arafa and M. M. Megahed, Evaluation of spur gear mesh compliance using the finite element method, Proc. IMechE, Part C: J. Mechanical Engineering Science, Vol. 213(6), pp.569-579,1999.

[6] A. L. Hedlund, "A parameterized numerical model for the evaluation of gear mesh stiffness variation of a helical gear pair," Proc. IMechE, Part C: J. Mechanical Engineering Science, Vol. 222(7), pp.1321-1327, 2008.

[7] J. M. Matusz, W. J. O'Donnel and R. J. Erdlac, "Local Flexibility Coefficients for the Built-in Ends of Beams and Plates," Journal of Engineering for Industry, pp. 607-614, 1969.

[8] Botman, M., "Epicyclic Gear Vibration," ASME J. Eng. Ind., Vol. 17, pp. 811-815, 1976.

[9] R. August and R. Kasuba , "Torsional Vibrations and Dynamic Loads in a Basic Planetary Gear System," J. Vib., Acoust. Stress Reliab. Des., Vol. 108, pp. 348-352, 1986.

[10] A. Kahraman, "Planetary gear train dynamics, " ASME J. Mech. Des., Vol. 116(3), pp. 713-720, 1994.

[11] P. Velex, and L. Flamand, , "Dynamic response of planetary trains to mesh parametric excitations, " ASME J. Mech. Des., 118(7), (1996), pp. 7-14.

[12] A. Saada and P.Velex, "An extended model for the analysis of the dynamic behavior of planetary trains, " ASME J. Mech. Des., Vol. 117(2), pp 141-247, 1995.

[13] J. Lin and R. G. Parker, "Analytical characterization of the unique properties of planetary gear free vibration," ASME J. Vibr. Acoust., Vol. 121(3), (1999), pp 316-321.

[14] Ambarisha,V. K., Parker, R. B. and Lin, J., "Suppression of planet mode response in planetary gear dynamics through meshing phasing, " ASME J. Mech. Des., Vol. 128(2), pp 133-142, 2004.

[15] A. Al-shyyab, and A. Kahraman, "A non-linear dynamic model for planetary gear sets," Proc. IMechE," Part K:: J. Multi-body Dynamics, Vol. 221(4), (2007), pp 567-576.

[16] A. Farshidianfar, H. Moeenfard, and Rafsanjani A., "Frequency response calculation of no nlinear torsional vibration in gear systems," Proc. IMechE, Part K: J. Multi-body Dynamics, Vol. 222(1), pp 49-60, 2008.

[17] R. Errichello, J. Muller, and M. Townsend, "Gearbox Reliability Collaborative Gearbox 1 Failure Analysis Report." NREL/SR-5000-53062, 2011.

About Authors:

Kuo Jao Huang: He is a professor of Department of Mechanical Engineering, Chung Hua University in Taiwan since 2011, but he has been a lecturer there since 1994. He got his degrees of MS in 1991 and PhD in 2002 both from Department of Mechanical Engineering of National Chiao Tung University. During 1991-1994, He was an associate researcher in MIRL, ITRI. His current research interests are: gear dynamics, gear design and manufacturing, computer aided design, and precision machine

Jeng Shiun Chen: He is a graduate student of Department of Mechanical Engineering, Chung Hua University (CHU). He also got the degree of BS in 2012 from CHU. Currently, his familiar field includes gear dynamics, gear design and manufacturing, computer aided design, and precision machine design.